Journal of Visualization, Vol. 8, No. 2 (2005)125-135

Visualization of Blast Waves Created by Exploding Bridge Wires

Murphy, M. J.*[1], Adrian, R. J.*[1], Stewart, D. S.*[1], Elliott, G. S.*[2], Thomas, K. A.*[3] and Kennedy, J. E.*[3]

*1 Laboratory for Turbulence and Complex Flow, Department of Theoretical & Applied Mechanics, University of Illinois, Urbana, IL, USA 61801
*2 Department of Aerospace Engineering, University of Illinois, Urbana, IL, USA 61801
*3 Los Alamos National Laboratory, Los Alamos, NM, USA 87545

Received 1 October 2004
Revised 29 November 2004

Abstract : Blast waves created by small exploding bridge wires are used as a test bed for the development of a particle image velocimetry (PIV) technique that uses polymers, seeded with scattering particles, as dynamic witness plates. Combined with pulsed, incoherent schlieren photography, the PIV method permits visualization of the instantaneous velocity vector field in a plane cutting through the blast wave.

Keywords : Exploding wires, Shock wave, Schlieren, Particle image velocimetry.

1. Introduction

Our initial studies have focused on exploding bridge wire (EBW) detonator devices. The flows they produce contain unsteady shock waves and high pressure and temperature gradients over micron to millimeter-sized length scales. Most characterizations of such micro-explosive flows are provided by numerical detonation wave theory, since experimental flow measurements are difficult due to the presence of high temperatures, high background luminance, and an inability to seed regions of interest with appropriate scattering particles. Thus, our motivation continues to be to develop valuable experimental techniques for making accurate high-speed flow measurements in explosive systems. We have used the EBW devices as a test bed for the development of high-speed flow diagnostics that permit visualization in such extreme environments. Specifically, we show visualization of EBW blast waves by pulsed, incoherent schlieren photography, by particle image velocimetry (PIV) in air, and by PIV in transparent, polymeric witness plates.

2. Exploding Bridge Wire Detonator

The EBW device currently in use is a model SE1 (BNC type) detonator provided by Los Alamos National Laboratory (LANL). The design consists of a 10 micron diameter gold wire, approximately 1.5 mm in length, attached to two electrical leads fixed atop the flat surface of a plastic cylindrical header. The detonator is operated by passing large amounts of electrical current across the bridge wire in very short time durations of typically less than one microsecond. The extremely rapid

transfer of electrical energy through the wire is commonly accomplished by capacitor discharge. With such rapid energy transfer times across the bridge wire, phase transitions from solid to liquid to gas are accomplished nearly instantaneously, while the wire geometry is maintained by inertia. Once wire vaporization overcomes inertia the energy is released through an explosion as heat and shock energy (RISI, 2000).

3. Pulsed Incoherent Schlieren Photography

The experimental setup is shown in Fig. 1. It is a standard schlieren system, except for the intense illumination device.

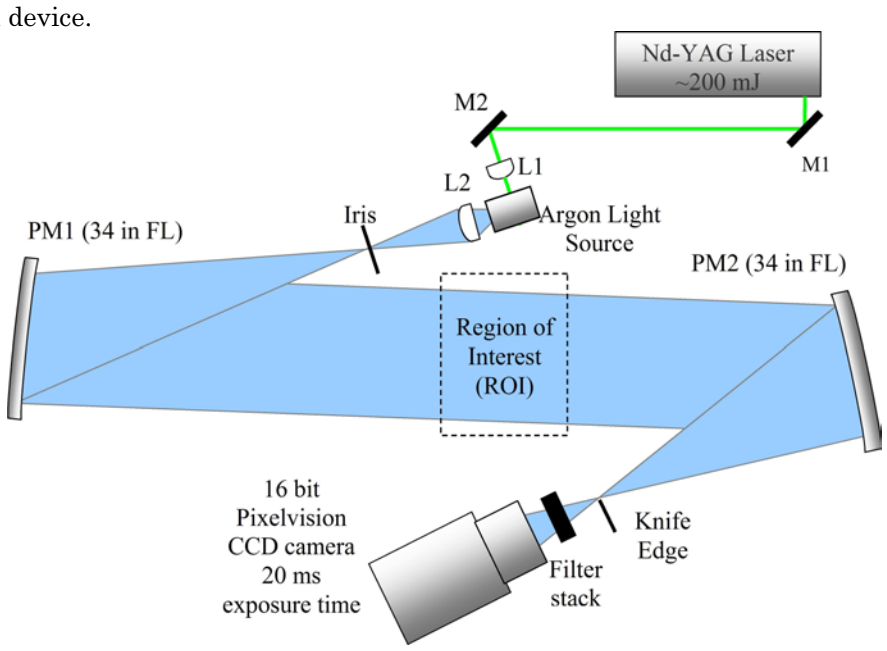

Fig. 1. Diagram of experimental Schlieren setup.

The EBW explosions emit bright light that must be substantially filtered to reduce pixel saturation on the charge-coupled device (CCD) chip in the camera. Consequently, the experiment requires an intense light source to backlight the explosions. To satisfy this need, an argon light source is employed which provides intense and incoherent backlighting.

The argon light source consists of an aluminum casing, which houses an internally fixed tungsten wire and an argon gas inlet. In operation, the chamber is pressurized with argon gas while a 200 mJ Nd-YAG laser beam (Continuum) is focused onto the tungsten wire. The visible light emitted from the aluminum chamber following each laser pulse results from laser-induced argon gas breakdown through multi-photon ionization of electrons ejected into the gas from the tungsten wire. The governing physics for this process are proposed in Evans and Gamal (1980).

With initial reference time, t_0, corresponding to the wire explosion, multiple instantaneous schlieren images are recorded for time intervals, Δt, ranging from 0.5 μs to 3 ms after the explosion. Two such images are displayed in Fig. 2 and are obtained by color filtering the original grayscale images.

The lead shock is clearly visible, as well as secondary shocks, baroclinic vorticity production at the header edges, and a buoyant plume of hot gas. With the axis of the EBW aligned normal to the camera axis, one notices the shock wave geometry is not spherical, as is expected since the physical geometry of the wire is cylindrical. Nonetheless, as the shock front travels greater distances away from the wire origin, one may expect the flow to approach a spherical geometry, as is depicted in Fig. 2 where Δt is 60 μs.

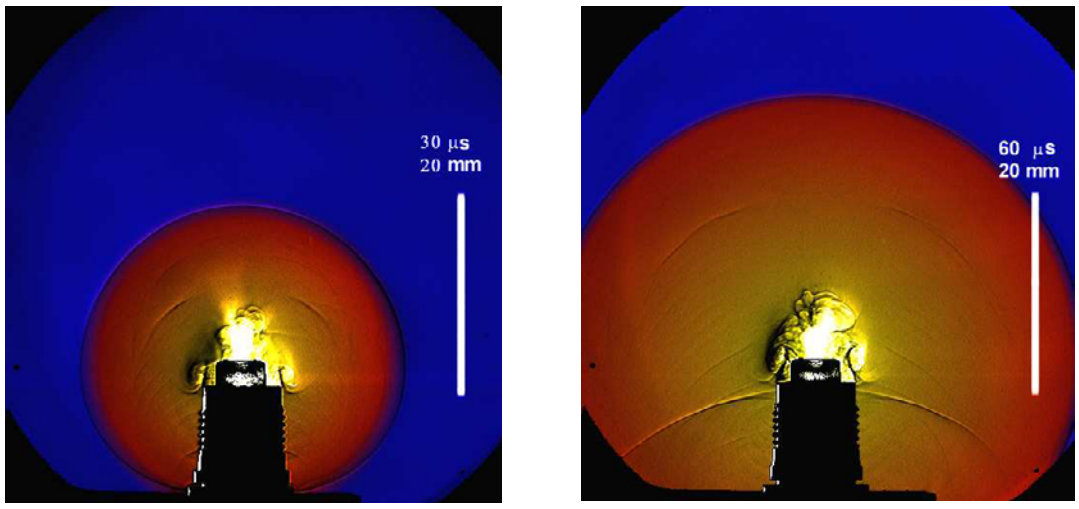

Fig. 2. Schlieren images with Δt = 30 μs and Δt = 60 μs for an input voltage of 3 kV. EBW is aligned perpendicular to camera axis.

Figure 3 displays two experimental images taken at time intervals of 2 μs and 4 μs respectively, with wire orientations parallel to the camera axis. By observing these images, it is apparent that the full three-dimensional flow field has both axisymmetric and non-axisymmetric geometries resembling the physical geometry of the bridge wire.

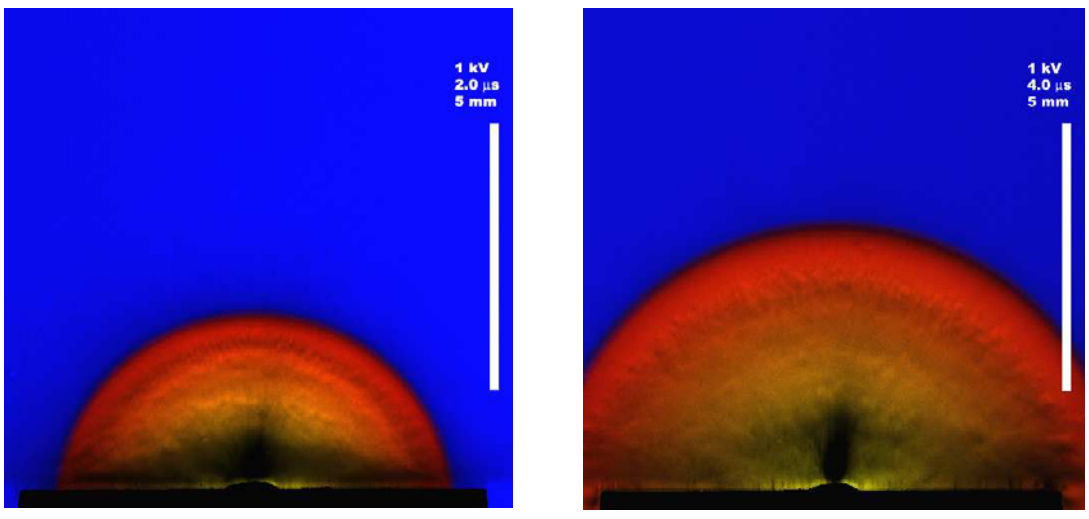

Fig. 3. Schlieren images with Δt = 2 μs and Δt = 4 μs for an input voltage of 1 kV. EBW is aligned parallel to camera axis.

From schlieren images recorded for times ranging from 0.5 μs to 60 μs, measurements of the position of the lead shock front are fit and the shock radius $R_S(t)$ is obtained as (see Fig. 4),

$$R_S(t) = 5.4488 t^{0.5394}. \quad (1)$$

The corresponding shock velocity is calculated as,

$$U_S(t) = \frac{dR_S(t)}{dt} = 2.93908\, t^{-0.4606}. \quad (2)$$

According to equation (2), the shock speed corresponding to our initial data point in Fig. 4 ($\Delta t = 0.5$ μs) is 2.35 km/s. The axisymmetric shock speeds corresponding to the images in Fig. 2 are 356 m/s and 258.7 m/s, respectively.

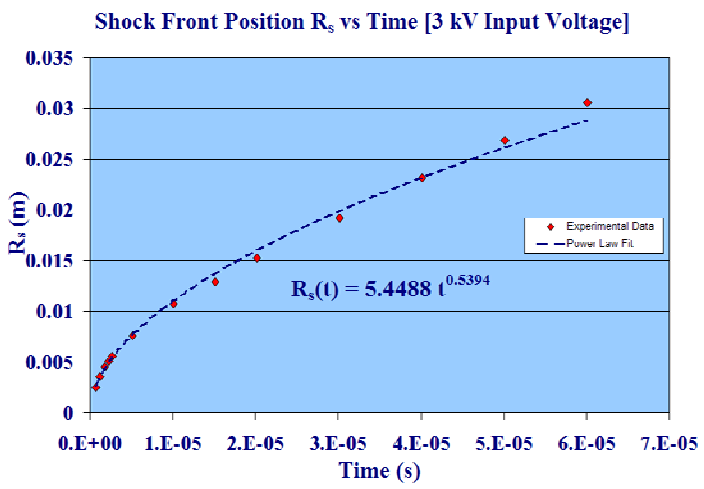

Fig. 4. Power-law fit for experimental shock position data points.

4. Compressible Flow Analysis

With a known function for shock velocity given by equation (2), as well as experimental evidence of an axisymmetric flow field arising from the cylindrical geometry of the bridge wire, it is possible to analytically calculate an induced particle velocity, *u*. This is accomplished by making a one-dimensional assumption that the axisymmetric shocks depicted in Fig. 3 are normal shocks, having a radius *Rs*, given by equation (1). Considering air as the working fluid and treating it as a diatomic, calorically perfect gas with an ideal equation of state, the compressible flow analysis involves a moving normal shock wave propagating into a quiescent fluid with ideal properties. If interested, the reader can consult a full analysis provided in Anderson (1990).

With undisturbed properties ahead of the shock designated by a "1" subscript, and disturbed properties behind the shock designated by a "2" subscript, the jump equations for pressure (*P*), temperature, (*T*), and density, (ρ), may be expressed as,

$$\frac{P_2}{P_1} = 1 + \frac{2\gamma}{\gamma+1}\left(M_S{}^2 - 1\right), \quad \frac{T_2}{T_1} = \frac{P_2}{P_1}\left(\frac{\frac{\gamma+1}{\gamma-1} + \frac{P_2}{P_1}}{1 + \frac{\gamma+1}{\gamma-1}\left(\frac{P_2}{P_1}\right)}\right), \quad \frac{\rho_2}{\rho_1} = \frac{1 + \frac{\gamma+1}{\gamma-1}\left(\frac{P_2}{P_1}\right)}{\frac{\gamma+1}{\gamma-1} + \frac{P_2}{P_1}}, \tag{3}$$

where *MS* is a shock mach number given by the ratio of shock speed *US* and sound speed ahead of the shock, a_1. Thus, with a known shock speed and ambient temperature measurement, the jump conditions can be determined, and the particle velocity behind the shock, *u*, can be obtained from continuity as,

$$u = U_S\left(1 - \frac{\rho_1}{\rho_2}\right). \tag{4}$$

5. Particle Image Velocimetry

Unlike schlieren, which can only measure the velocity of the shock waves, PIV offers the possibility of visualizing the material velocity continuously on a plane defined by a laser light sheet. In principle, the application of PIV to fast, high pressure gas flows is straight forward. However, one must contend

with the fact that seed particle velocities may lag the fluid material velocity, owing to the inertia of the particles and the enormous values of the accelerations across the shock waves. For example, considering a typical 1,000 m/s shock wave in air at 298 K, the velocity drops by 267 m/s across the 16 nm shock wave (Granger, 1985), corresponding to an acceleration of 4.45×10^{12} m/s^2. Thus, the type of particle used and its dynamic behavior in rapidly varying flows are critical issues for successful application of PIV.

In this work, our interest is in making the first demonstration of the feasibility of applying PIV to blast waves and in assessing the magnitude of the particle lag errors for simple oil droplet aerosols. With theoretical particle velocities in air obtainable through compressible flow analysis, PIV data provides an experimental means of determining particle lag velocities given by $|\boldsymbol{v_p} - \boldsymbol{u}|$, and hence particle Reynolds numbers Re_p, in terms of $\boldsymbol{v_p}$, where $\boldsymbol{v_p}$ denotes particulate velocity.

5.1 PIV in Air

An atomizer utilizing a Laskin-nozzle design is employed to produce 1-2 μm diameter olive oil particles to function as individual light-scattering markers in the fluid flows. A high-density aerosol of particles is continuously injected into the immediate surroundings of an EBW header resulting in a region of particle-seeded air approximately 27 cm^3 in dimension. A 50 mJ Nd-YAG laser (New Wave MiniLase III) provides particle illumination with pulse durations of 5-7 ns, while the images are captured using an 8-bit, TSI CCD camera (10-30 PIVCAM) with *1* Mpixel resolution. The camera is operated in a dual exposure, frame-straddle mode allowing two-frame cross-correlation analysis to be used with one laser pulse fired within each camera exposure.

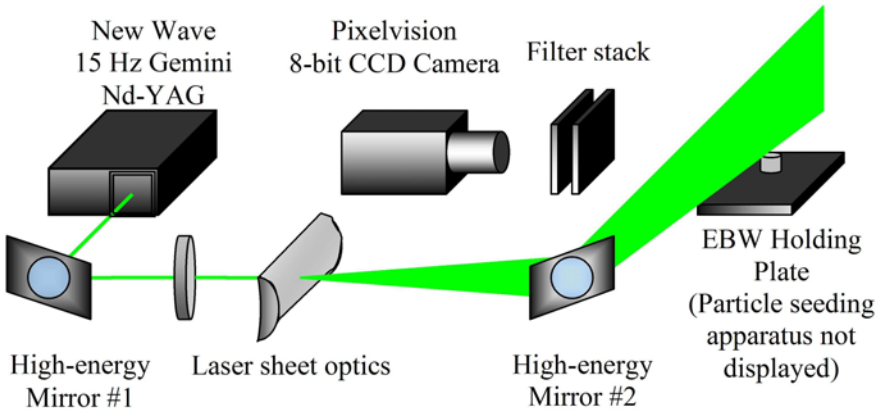

Fig. 5. PIV experimental setup for EBW blasts in air.

The PIV timing parameters governing laser pulse firing, pulse separation, camera delay and data acquisition times are all controlled by a TSI LaserPulse synchronizer (model 610034). In order to accurately trigger the synchronizer and EBW electronics to within nanoseconds, the entire experiment is triggered with a BNC pulse generator (555 series) functioning as the timing master.

Experiments are conducted with event times (ET) in the range of 7 μs to 20 μs, with a fixed laser pulse separation time, dT, of 2 μs. The event time refers to the time between wire explosion and the first laser pulse. The camera and EBW axes have been aligned to exploit the axisymmetric flow geometry, resulting in particulate velocities, $\boldsymbol{v_p}$ that are assumed radial for this analysis. Figures 6 and 7 display two experimental vector fields obtained for total time T, equal to 19.5 μs and 22 μs, respectively, where $T = ET + dT$.

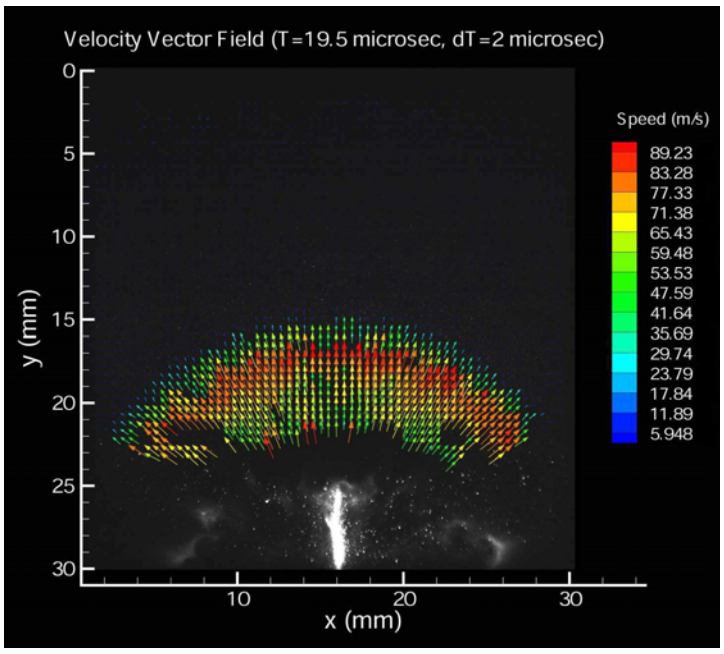

Fig. 6. Velocity field obtained for T = 19.5 μs.

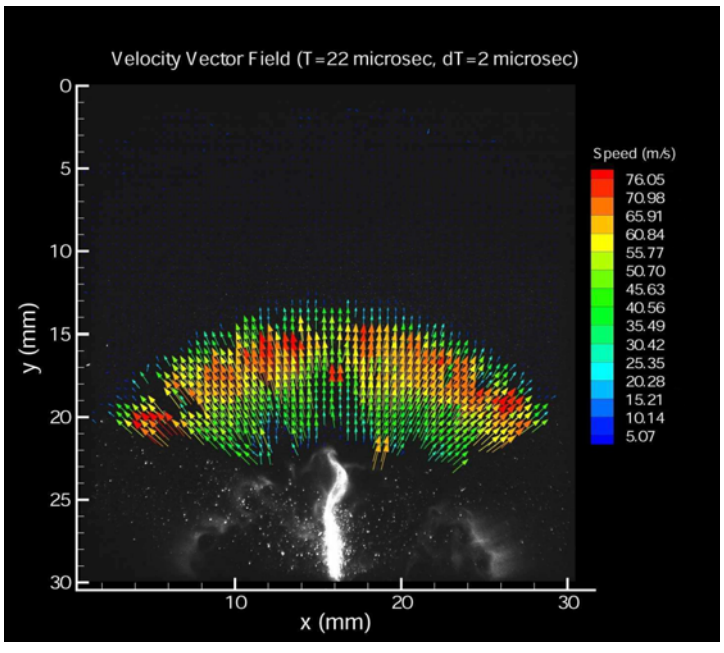

Fig. 7. Velocity field obtained for T = 22μs.

By using plots of velocity contours from PIV data to determine average velocities at multiple r values, where r denotes radial distance, particulate velocity measurements as a function of radial distance away from the EBW are obtained. The plots of $\boldsymbol{v_p}$ versus r corresponding to the vector fields in Figs. 6 and 7 are shown in Fig. 8.

Considering the case for $T = 22$ μs, the maximum particulate velocity measured from PIV data is $|\boldsymbol{v_p}| = 73.5$ m/s. Equation (2) gives a shock velocity of 410.7 m/s, resulting in a Mach number of 1.185. Evaluating the jump conditions, and using an ambient air temperature of 298.67 K, gives a particle velocity of $|\boldsymbol{u}| = 98.707$ m/s, and hence a lag velocity of $|\boldsymbol{v_p} - \boldsymbol{u}| = 25.21$ m/s. Notice a lag distance of approximately 1-2 mm is necessary for the particulate velocity to reach its maximum value, as depicted in Fig. 8. This suggests a large particle lag exists within the flow measurements.

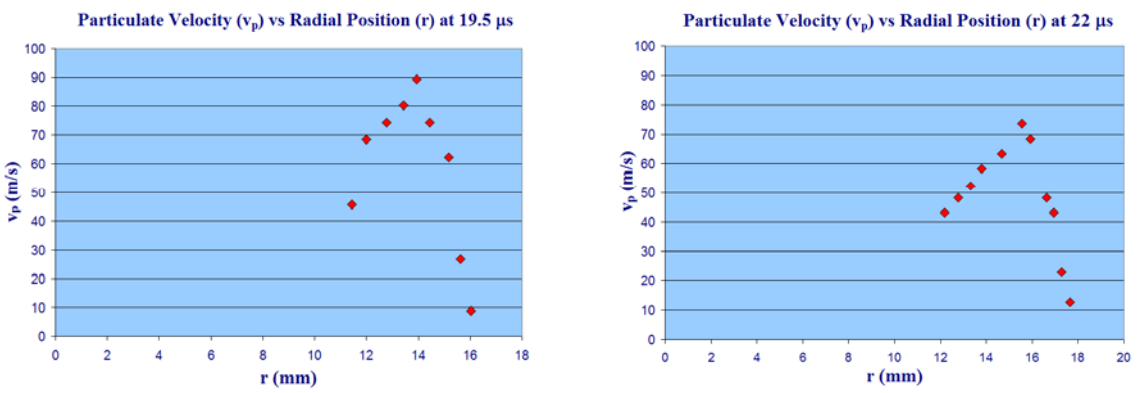

Fig. 8. Plots of particulate velocity versus radial distance for T = 19.5 µs (left) and 22 µs (right).

5.1.1 Analysis of Particle Dynamics

Concerning particle response, an approximate particle dynamic equation governing a single liquid particle suspended in a gas is provided in Adrian (1991) as,

$$\left(\rho_p \frac{\pi}{6} d_p^{\,3}\right)\frac{d\boldsymbol{v}_p}{dt} = C_D \rho \frac{\pi}{4} d_p^{\,2} \left|\boldsymbol{v}_p - \boldsymbol{u}\right|\left(\boldsymbol{v}_p - \boldsymbol{u}\right), \tag{5}$$

where the right-hand side has been simplified to a static drag law contribution with drag coefficient, C_D. Terms with a "p" subscript denote particulate properties. The above simplification is made under the condition that momentum contributions from added fluid mass, unsteady drag forces, external pressure gradients, and other forces provide negligible corrections when compared with drag on the particle. Solving equation (5) for the particle lag velocity gives

$$\left|\boldsymbol{v}_p - \boldsymbol{u}\right| = \left(\frac{2}{3}\frac{\rho_p}{\rho}\frac{d_p}{C_D}\left|\frac{d\boldsymbol{v}_p}{dt}\right|\right)^{1/2}. \tag{6}$$

Then, a particle Reynolds number may be defined as

$$\mathrm{Re}_p = \frac{\left|\boldsymbol{v}_p - \boldsymbol{u}\right| d_p}{\nu}. \tag{7}$$

In the limit $\mathrm{Re_p} << 1$, the drag on the particle can be characterized by Stokes' law, which gives

$$F_D = 6\pi\mu\left(\frac{d_p}{2}\right)\left|\boldsymbol{v}_p - \boldsymbol{u}\right|. \tag{8}$$

By equating the right-hand side of equation (5) with equation (8), C_D may be evaluated. Furthermore, equating the left-hand side of equation (5) with equation (8) and solving for particle acceleration yields

$$\frac{d\boldsymbol{v}_p}{dt} = \left(\frac{18\rho\nu}{\rho_p d_p^{\,2}}\right)\left|\boldsymbol{v}_p - \boldsymbol{u}\right| = \frac{\left|\boldsymbol{v}_p - \boldsymbol{u}\right|}{\tau_\mathbf{p}}, \tag{9}$$

where τ_p represents the particle lag time which scales with particle diameter as d_p^2. Thus, within the validity of Stokes' law analysis, reducing seed particle size should greatly improve particle response times. Alternatively, if $\mathrm{Re_p} \sim O(1)$ or greater, then a nonlinear drag law is necessary.

Referring back to the flows depicted in Figs. 6 and 7, the lag velocities calculated for $T = 19.5$ µs and 22 µs are 42.19 m/s and 25.21 m/s, respectively. Since the viscosity (ν) of air at 298 K is 1.6×10^{-5} m^2/s, and the particle diameter is approximately *1* µm, then the corresponding Reynolds numbers are 2.637 and 1.575. These values suggest a complex nonlinear drag law is necessary, due to the presence of large particle lag velocities.

It is important to note that a definite minimum particle diameter exists after which smaller diameter particles cannot scatter enough laser light intensity for accurate PIV measurements to be

made. A thorough discussion of this situation is presented in Adrian and Yao (1985), wherein an approximate minimum particle diameter is suggested as 0.5 μm.

5.2 PIV in Solid Polydimethylsiloxane (PDMS)

An alternative method for visualizing high-speed disturbances caused by shock waves involves observing a disturbance as it propagates through a solid with known shock properties. In this manner, the known characteristics of the surrounding medium allow one to characterize the disturbances in question. With this is mind the silicone polymer polydimethylsiloxane (PDMS), known commercially as Sylgard, is seeded with light-scattering particles. PIV measurements are then made of propagating disturbances caused by applied explosive loads from EBW detonator blasts in particle-seeded PDMS samples.

An experimental study of the shock characteristics of "Sylgard 184 ®", i.e. experimental and numerical comparisons of the principal Hugoniot, a parameter fit of the governing equation of state (EOS), and a sound speed, *a*, given as 1.63 mm/μs, can be found in Winter et al. (2003). As for the seed particles, polymer samples have been seeded with 4 μm diameter, metallic-coated polystyrene particles in a fixed concentration of 10 particles per 100 μm^3. Though it is not the case with the polystyrene particles used in this experiment, it is possible to match the acoustic properties of the seed particles with those of the polymer, such that issues concerning the effects of seed particles on material-specific parameters in the governing EOS may be alleviated.

The PIV setup used for measuring the induced particle velocities in air has been utilized for this experiment as well, with a mounting attachment added to accurately hold the polymer samples directly above the EBW devices. Preliminary experiments have been completed for event times ranging from 2 μs to 15 μs following wire explosion. A fixed input voltage of 3.02 kV is used, as well as a fixed laser pulse separation time of 2 μs. Figure 9 shows a mean particle displacement field taken 7 μs after EBW explosion in support of the experimental accuracy with which particle displacements can be obtained from moving seed particles illuminated in a solid polymer.

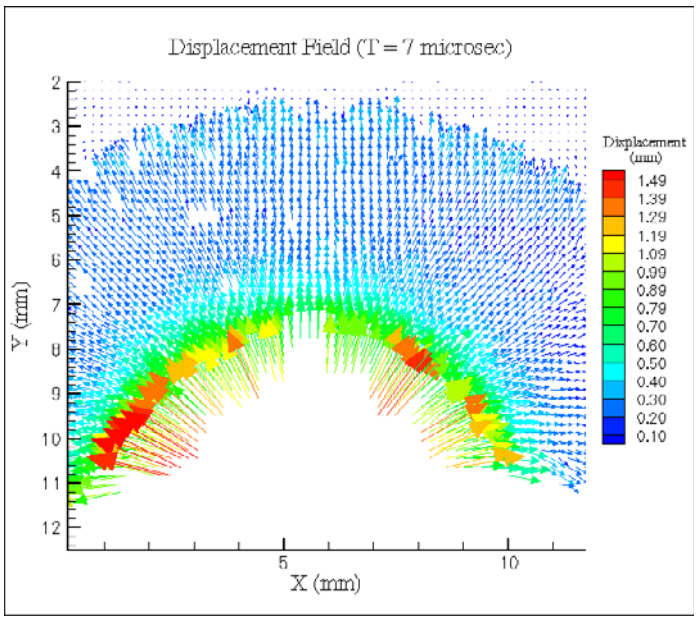

Fig. 9. Mean particle displacement field obtained 7 μs after wire explosion.

Two velocity vector fields are shown in Figs. 10 and 11 with corresponding event times of 5 μs and 6 μs, respectively. By observing these vector fields the improved particle response is evident by noticing the distinct boundary between the disturbed and undisturbed regions of the sample, corresponding to the propagating disturbance. There are also noticeable regions in the center of the

flow fields where the velocity vectors have nearly zero magnitude or are pointing in a direction opposite to the propagation direction of the disturbance. These regions in the vector fields suggest expansion waves may be adversely propagating directly behind the disturbances in a similar manner as in gas flows, where expansion waves propagate adversely behind shocks. Because of these observations, future PIV experiments involving shocks will contain simultaneous schlieren images of the same flow field, such that pressure gradients may be directly identified and compared with corresponding velocity vector fields. Figure 12 shows a color filtered schlieren image of an EBW-induced disturbance propagating in a PDMS sample 20 μs after wire explosion.

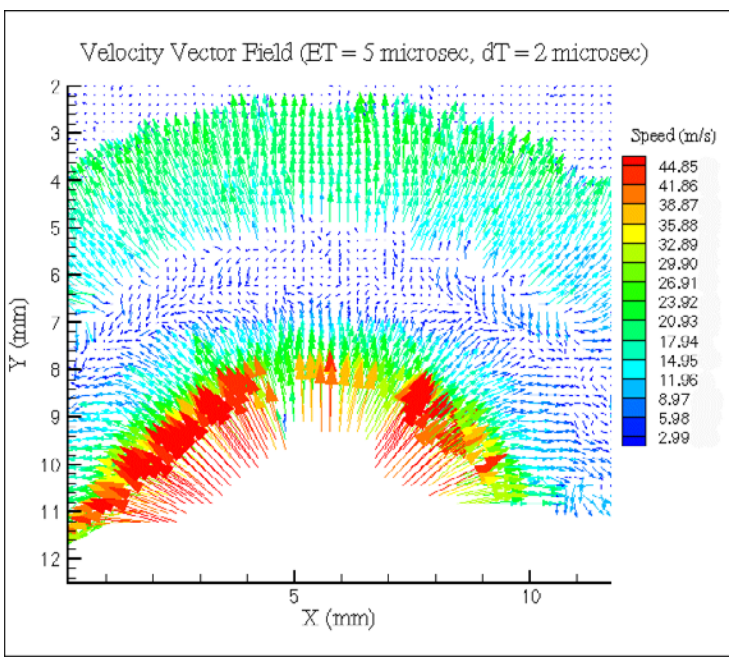

Fig. 10. Velocity vector field obtained 7 μs after wire explosion.

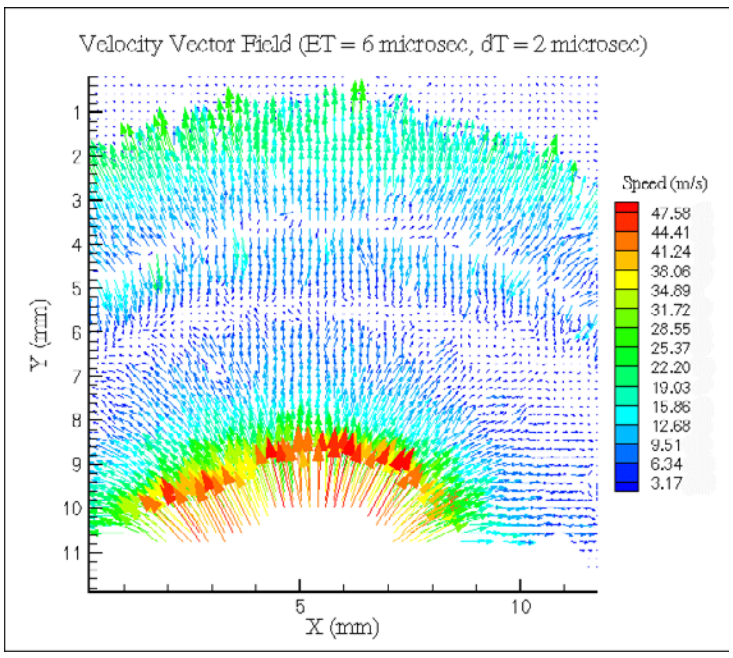

Fig. 11. Velocity vector field obtained 8 μs after wire explosion.

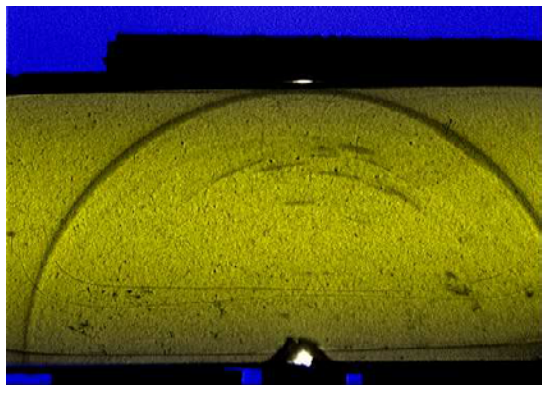

Fig. 12. Schlieren of disturbance propagating through a PDMS sample.

6. Summary

In this work we show that pulsed, incoherent schlieren photography is successfully applied to flow fields caused by exploding bridge wire (EBW) detonators. The experimental schlieren images provide useful details about flow characteristics, such as evidence of axisymmetric flow geometry and mathematical expressions for shock position and shock velocity with respect to time. With measured explosive shock speeds up to 2 km/s, the high-speed, unsteady shocks induce large particle velocities in the ambient air into which they propagate. Analytical calculations for particle velocities of this type are obtained from appropriate compressible flow analysis.

PIV measurements of the induced particle velocities yield particulate velocities which strongly lag mean flow speeds, resulting in poor particle response. In principle, reducing the seed particle diameter should provide one possible corrective measure for reducing particle lag velocities in high speed flows. A second corrective measure involves an extension of PIV measurements to particle-seeded PDMS samples, where the known shock properties of the samples allow them to be utilized as dynamic witness plates for shock-induced flows. Thus, the principal goal of successful flow measurements of a micro-explosive system, as well as an improvement of particle response, is demonstrated for EBW-induced flows.

Acknowledgement

This research is supported by the Los Alamos National Laboratory and US Department of Energy, Contract # 3223501019Z.

References

Adrian, R. J., Particle-imaging techniques for experimental fluid mechanics, Ann. Rev. Fluid Mech., 23 (1991), 261-268.
Adrian, R. J. and Yao, C. S., Pulsed laser technique application to liquid and gaseous flows and the scattering power of seed materials, Applied Optics, 24-44 (1985), 47-50.
Anderson, J. D., Modern compressible flow (2nd ed.), (1990), 206-213, McGraw-Hill.
Bennett, F. D., Flow Fields Produced by Exploding Wires, 1 (1959), 211-226, Plenum Press Inc., New York.
Evans, C. J. and Gamal, Y. E., J. Phys. D: Appl. Phys. B (1980), 1447-1458.
Granger, R. A., Fluid Mechanics, (1985), 845, Holt, Rinehart, and Winston, New York.
Lin, S. C., Cylindrical Shock Waves Produced by Instantaneous Energy Release, J. Appl. Phys., 25-54 (1954).
Reynolds Industries, Incorporated (RISI). Exploding bridgewire (EBW) detonators. www.risi-usa.com (2000).
Sakurai, A., On the Propagation and Structure of the Blast Wave, I. J. Phys. Soc. of Japan, 8- 5 (1958), 662-669.
Winter, R. E., Whiteman, G., Haining, G. S., Salisbury, D. A. and Tsembelis, K., Measurement of equation of state of silicone elastomer, (2003), British Crown.

Author Profile

Michael J. Murphy: He received his B.S. degree in Physics in 2002 from California State University Stanislaus and is currently completing his M.S. degree in the Department of Theoretical and Applied Mechanics under the advisement of Ronald J. Adrian at the University of Illinois. His research interests are micro-detonations, compressible flows, experimental optics, and experimental fluid mechanics using optical techniques such as holography, schlieren photography, and particle image velocimetry.

Ronald J. Adrian: He received his B.M.E. degree in Mechanical Engineering in 1967 from the University of Minnesota, his M.S. degree in Mechanical Engineering in 1969 from the University of Minnesota, and his Ph.D. degree in Physics in 1972 from the University of Cambridge. He joined the University of Illinois in 1972 where he became a full Professor in 1981. He now holds the Leonard C. and Mary Lou Hoeft Chair in Engineering and is Director of the Laboratory on Turbulence and Complex Flows in the Department of Theoretical and Applied Mechanics. His research interests are turbulence, wall turbulence, thermal convection, vortex structures, laser instrumentation and experimental fluid mechanics.

D. Scott Stewart: He obtained a BS.E. at the University of New York at Buffalo, Engineering Science in 1976 and his Ph. D. in Theoretical and Applied Mechanics, Cornell University in 1981. He joined Theoretical and Applied Mechanics, University of Illinois in 1981 and is a full professor. His work has been generously supported by Los Alamos National Laboratory and the U.S. Air Force in the areas of reactive flow, shock physics, modeling, advanced simulation and miniaturization of explosive technology. He is a fellow of the American Physical Society, Institute of Physics and Associate Fellow of AIAA.

Greg Elliott: He received his M.Sc. (Eng) in Mechanical Engineering in 1989 from The Ohio State University. He also received his Ph.D. in Mechanical Engineering in 1993 from The Ohio State University. After a two-year post-doc he joined the Department of mechanical and Aerospace Engineering at Rutgers University as an assistant professor in 1995 and was promoted to associate professor in 2000. In 2003 he joined the faculty of the Aerospace Engineering Department at the University of Illinois at Urbana-Champaign as an associate professor. His research interests include the development of laser diagnostics, experimental fluid mechanics, compressible flow, turbulence, combustion, and plasmas.